Pharmaceutical Research (2023) 40:2791–2800
https://doi.org/10.1007/s11095-023-03533-w

ORIGINAL RESEARCH ARTICLE

Modulating Pharmaceutical Properties of Berberine Chloride through Cocrystallization with Benzendiol Isomers

Hongjie Guo[1] · Shuyu Liu[1] · Changquan Calvin Sun[2]

Received: 28 March 2023 / Accepted: 10 May 2023 / Published online: 24 May 2023

Abstract

Purpose To synthesize and characterize new cocrystals of berberine chloride (BCl) for potential pharmaceutical tablet formulation.

Methods Solutions of BCl with each of three selected cocrystal formers, catechol (CAT), resorcinol (RES), and hydroquinone (HYQ) were slowly evaporated at room temperature to obtain crystals. Crystal structures were solved using single crystal X-ray diffraction. Bulk powders were characterized by powder X-ray diffraction, thermogravimetric-differential scanning calorimetry, FTIR, dynamic moisture sorption, and dissolution (both intrinsic and powder).

Results Single crystal structures confirmed the formation of cocrystals with all three coformers, which revealed various intermolecular interactions that stabilized crystal lattices, including O–H···Cl^- hydrogen bonds. All three cocrystals exhibited better stability against high humidity (up to 95% relative humidity) at 25 ℃ and higher intrinsic and powder dissolution rates than BCl.

Conclusion The enhanced pharmaceutical properties of all three cocrystals, as compared to BCl, further contribute to the existing evidence that confirms the beneficial role of cocrystallization in facilitating drug development. These new cocrystals expand the structure landscape of BCl solid forms, which is important for future analysis to establish a reliable relationship between crystal structure and pharmaceutical properties.

Keywords berberine · cocrystallization · dissolution · soubility · stability

Introduction

Cocrystallization is an effective crystal engineering approach for improving the solid-state properties of active pharmaceutical ingredients (APIs), such as solubility, dissolution, bioavailability, and stability, without changing their pharmacological activities [1–6]. Cocrystals can be synthesized under relatively mild conditions, such as at room temperature by grinding [7, 8]. However, It is not yet possible to reliably design cocrystals with desired product performance [9, 10]. Attaining such a goal requires a robust understanding of the crystal structure and property relationship [11], which demands a large number of cocrystals with pertaining properties characterized.

Berberine (Fig. 1a) is a compound with anti-bacterial and anti-inflammatory activities [12, 13]. Berberine has the effects of dilating blood vessels and reducing blood pressure and thrombosis [14, 15]. Corresponding to these potential clinical benefits, berberine has been used to treat ventricular arrhythmia and supraventricular arrhythmia [16]. Given its pharmaceutical importance, several cocrystals of its chloride salt, BCl, have been prepared to modify its properties [17–21], making it one of possible candidate systems for exploring an understanding of crystal structure – property relationship. Among the pharmaceutical properties, we are mainly interested in solubility and dissolution because the ability to modulate solubility and dissolution is important for attaining adequate bioavailability of poorly soluble APIs, such as berberine. The solubility of BCl·2H2O in water is 3.27 mg/mL at 37°C [22]. Despite a predicted pK_a value of -4.4 was report in

✉ Shuyu Liu
liushuyu1219@163.com

✉ Changquan Calvin Sun
sunx0053@umn.edu

[1] School of Chemistry and Chemical Engineering, Shanghai University of Engineering Science, Shanghai 201620, China

[2] Pharmaceutical Materials Science and Engineering Laboratory, Department of Pharmaceutics, University of Minnesota, Minneapolis, MN 55455, USA

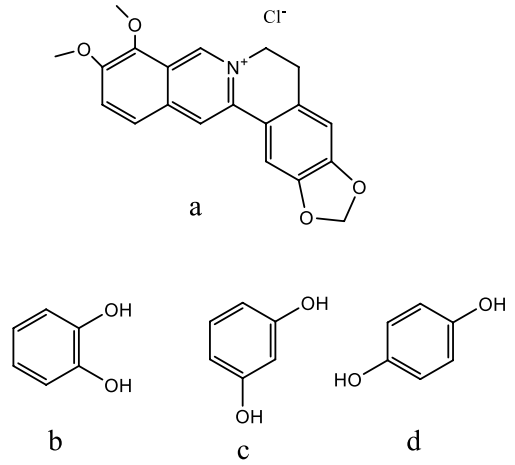

Fig. 1 Chemical structures of (**a**) berberine chloride (BCl), (**b**) catechol (CAT), (**c**) resorcinol (RES), (d) hydroquinone (HYQ).

the DrugBank, the concept of pK_a is not applicable to berberine because it is a quaternary ammonium compound with a permanent positive charge, where a proton is not involved in its ionic equilibrium. The log *P* value predicted by Chemaxon in the DrugBank is -1.3. Globally, the aqueous solubility of cocrystals positively correlates with that of coformer, if cocrystals do not undergo phase change during equilibrium with a saturated solution [23–28]. We previously found that the cocrystals of BCl with aliphatic dicarboxylic acids exhibited odd-even alternation in melting points and intrinsic dissolution rates with the carbon chain length [19]. In three BCl cocrystals prepared with aromatic carboxylic acids, namely, 4-aminobenzoic acid, 4-hydroxybenzoic acid and 2,6-dihydroxybenzoic acid, an inverse relationship between melting point and dissolution rate was found [20].

In this work, we have prepared three new cocrystals of BCl with structurally similar benzendiol isomers (Fig. 1b–d), i.e., catechol (CAT), resorcinol (RES), and hydroquinone (HYQ), to further increase the chemical diversity of BCl cocrystals. Benzendiol coformers were previously shown to improve the physicochemical properties of some APIs [26, 29–32]. They all have high aqueous solubility, which make them attractive candidates for synthesizing cocrystals with improved solubility.

Materials and Methods

Materials

Berberine chloride dihydrate (BCl·2H_2O, 97% purity) were purchased from Shanghai Civi Chemical Co., Ltd. (Shanghai, China). Catechol (CAT, 99% purity), resorcinol (RES, 99% purity) and hydroquinone (HYQ, 99% purity) were purchased from Shanghai Titan Scientifical Co., Ltd. (Shanghai, China). All materials were used as received.

Methods

Preparation of BCl Cocrystals

Three cocrystals of BCl, i.e., BCl-CAT·H_2O, BCl-RES and BCl-HYQ·$CHCl_3$, were prepared by slow solvent evaporation. BCl·2H_2O (20 mg, 0.049 mmol) and CAT (5.4 mg, 0.049 mmol) were dissolved in 2 mL methanol. The solution was allowed to evaporate slowly at room temperature. Yellow crystals were obtained after 3 days. Yellow crystals of BCl-RES and BCl-HYQ·$CHCl_3$ were obtained in a similar manner but using a chloroform-methanol mixture (v:v = 10:1) as a solvent. Several parallel reactions were set up under identical conditions to prepare multiple cocrystal samples, which were combined to obtain bulk powders for characterization.

Single Crystal X-ray Diffraction (SCXRD)

Single crystal X-ray diffraction data were collected on a Bruker APEX-II CCD diffractometer (Karlsruhe, German). Crystal structures were solved by direct methods and optimized with full-matrix least squares method on F^2 using ShelXT program. All non-hydrogen atoms were refined anisotropically. All hydrogen atoms were refined isotropically.

Powder X-ray Diffraction (PXRD)

PXRD were carried out on a Bruker D8 Advance powder diffractometer with a Cu-K_α radiation at room temperature.

Table I Crystallographic Data of Berberine Chloride Cocrystals

	BCl-CAT·H_2O	BCl-RES	BCl-HYQ·$CHCl_3$
Empirical formula	$C_{26}H_{26}ClNO_7$	$C_{26}H_{24}ClNO_6$	$C_{27}H_{25}Cl_4NO_6$
Formula weight	499.93	481.91	601.28
Temperature/K	170	170	170
Crystal system	monoclinic	triclinic	triclinic
Space group	$P2_1/n$	P-1	P-1
a/Å	17.4771(17)	9.962(2)	7.4595(19)
b/Å	7.2961(6)	10.527(2)	14.587(3)
c/Å	19.3333(18)	12.651(3)	25.793(6)
α/°	90	76.807(7)	100.988(9)
β/°	109.592(3)	69.278(7)	93.653(9)
γ/°	90	64.412(6)	95.301(9)
volume/$Å^3$	2322.55(37)	1976.7(3)	2733.8(11)
Z	4	2	4
ρ(calc)/g •cm^{-3}	1.430	1.436	1.461
CCDC	2236536	2236537	2236538

The current and voltage were 40 mA and 40 kV, respectively. PXRD data was collected in the 2θ range of 5–45° with a scanning speed of 10°/min.

Thermal analyses

The thermogravimetric analysis (TGA) and differential scanning calorimetry (DSC) thermograms of BCl·2H_2O and the three cocrystals were simultaneously determined by a STA-8000 thermal analyzer (PerkinElmer, USA). Each sample (5 ~ 10 mg) was placed in an aluminum pan and heated from 30 to 250℃ under nitrogen at a heating rate of 10℃/min.

Fourier Transformation Infrared Spectroscopy (FT-IR)

FT-IR spectra of all samples were collected on a FTIR spectrophotometer (Nicolet iS20, Thermo Scientific) using KBr pellets at room temperature. Samples were scanned in the wavenumber range of 4000 to 400 cm^{-1} with the resolution of 4 cm^{-1}, each spectrum is an average of 32 scans.

Dynamic Water Vapor Sorption Isotherm (DVS)

Moisture sorption properties of these samples were measured using a DVS instrument (Intrinsic, Surface Measurement Systems, London, UK) at 25 ± 0.1℃. The mass change of the samples was monitored over a humidity cycle of 0–95–0% RH in 10% RH steps up to 90% RH and then 5% step to 95% RH under a continuous flow of nitrogen with a desired RH at each step. An equilibration criterion of dm/dt < 0.002% min^{-1} was applied for all steps. The Samples were assessed by PXRD before and after each DVS experiment to detect possible phase change.

High Performance Liquid Chromatography (HPLC) Analysis

The concentration of berberine were determined on an HPLC (LC-1260S, Agilent) equipped with a C18 column (4.6 mm × 150 nm, 5 μm). A mixture of methanol and 0.4% phosphoric acid (40/60, v/v) was used as the mobile phase with the flow rate of 1.0 mL/min at 30℃. The detection wavelength was 230 nm and the injection volume of sample was 10 μL.

Accurately weighed BCl·2H_2O was dissolved in volumetric flasks to obtain standard solutions with approximate concentrations of 0.01, 0.02, 0.05, 0.10, 0.13, 0.17, 0.22, and 0.25 mg/mL. Linear regression of the peak area of berberine (Y) *vs.* concentration (X, mg/mL) led to a standard curve of Y = 42680X (R^2 = 0.9999), which conformed to the analysis requirement.

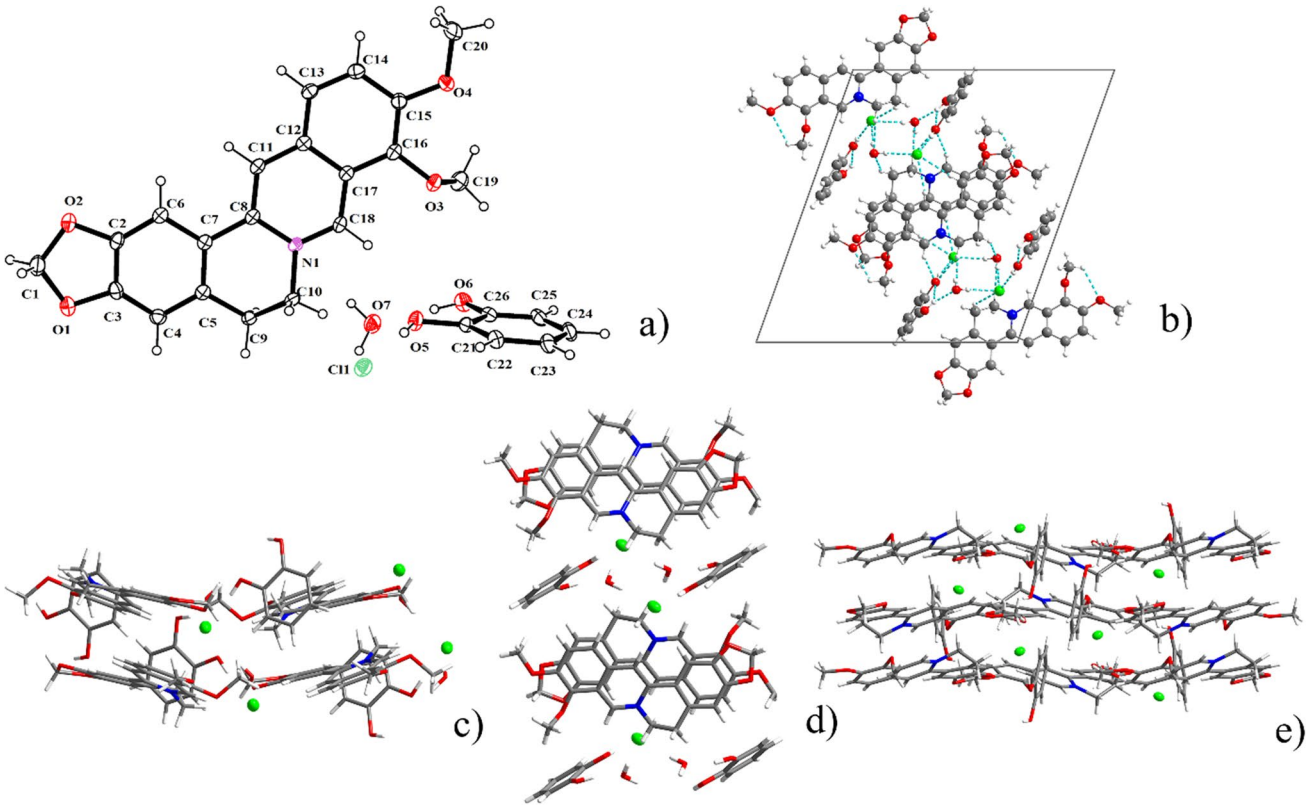

Fig. 2 The crystal structure of BCl-CAT·H_2O, (**a**) ORTEP diagram with labelling scheme, (**b**) key intermolecular interactions (hydrogen bonds are teal colored), and molecular packing viewed along (**c**) *a*-axis, (**d**) *b*-axis, and (**e**) *c*-axis.

Solubility

Aqueous solubility was determined by the shake-flask method. Approximately 100 mg of each sample was suspended in 5 mL deionized water, and was magnetically stirred at 37℃ for 24 h. The suspension was then filtered through a 0.25 μm Nylon filter. After discarding the first two drops, the filtered solution collected with the concentration of BCl determined by HPLC. The solubility of each sample was tested in triplicate and remaining solids were analyzed by PXRD for phase identification.

Intrinsic Dissolution Rates (IDR)

IDR was measured by using a compressed disc (12 mm diameter, 250 mg) on an infrared tablet press (FW-5A, Tianjin Botian Shengda, China) at 15 MPa hydraulic pressure for 3 min. The side and one face of the disc was coated with beeswax, so that only one flat surface was exposed to the dissolution medium. The disc was introduced into a dissolution vessel containing 900 mL distilled water. The temperature of the water bath was 37℃ and the stirring rate was 50 rpm. Concentration of BCl in the dissolution medium at 1, 4, 7, 10, 15, 20, 25, 30, 40, 50, and 60 min was determined by HPLC. At each time point, 5 mL of the medium was withdrawn and the same volume of fresh dissolution medium was immediately added. Before HPLC analysis, the solution was filtered through a 0.22 μm Nylon filter. After discarding the first two drops, the filtered solution was collected and diluted as appropriate for concentration determination. The determination of IDR of each cocrystal was triplicated.

Powder Dissolution

BCl·2H_2O, BCl-CAT·H_2O, BCl-RES and BCl-HYQ·$CHCl_3$ powders were manually ground in a mortar and sieved with a 100-mesh sieve before the dissolution experiment. In each run, an accurately weighed sample corresponding to approximately 100 mg of BCl was placed in the dissolution vessel containing 900 mL distilled water. The temperature of the water bath was 37℃ and the stirring rate was 50 rpm. Concentrations of BCl at 5, 10, 15, 20, 30, 45, 60, 90, 120 min were determined the same way as that for IDR determination.

Results and Discussion

Crystal Structure Analysis

The key crystallographic data of the three cocrystals of BCl are listed in Table I. Both BCl-HYQ·$CHCl_3$ and BCl-RES crystals belong to the triclinic P-1 space group, while BCl-CAT·H_2O belongs to the monoclinic P21/n space group.

The asymmetric unit of the BCl-CAT·H_2O contains one BCl, one CAT, and one H_2O (Fig. 2a). Berberine cations and

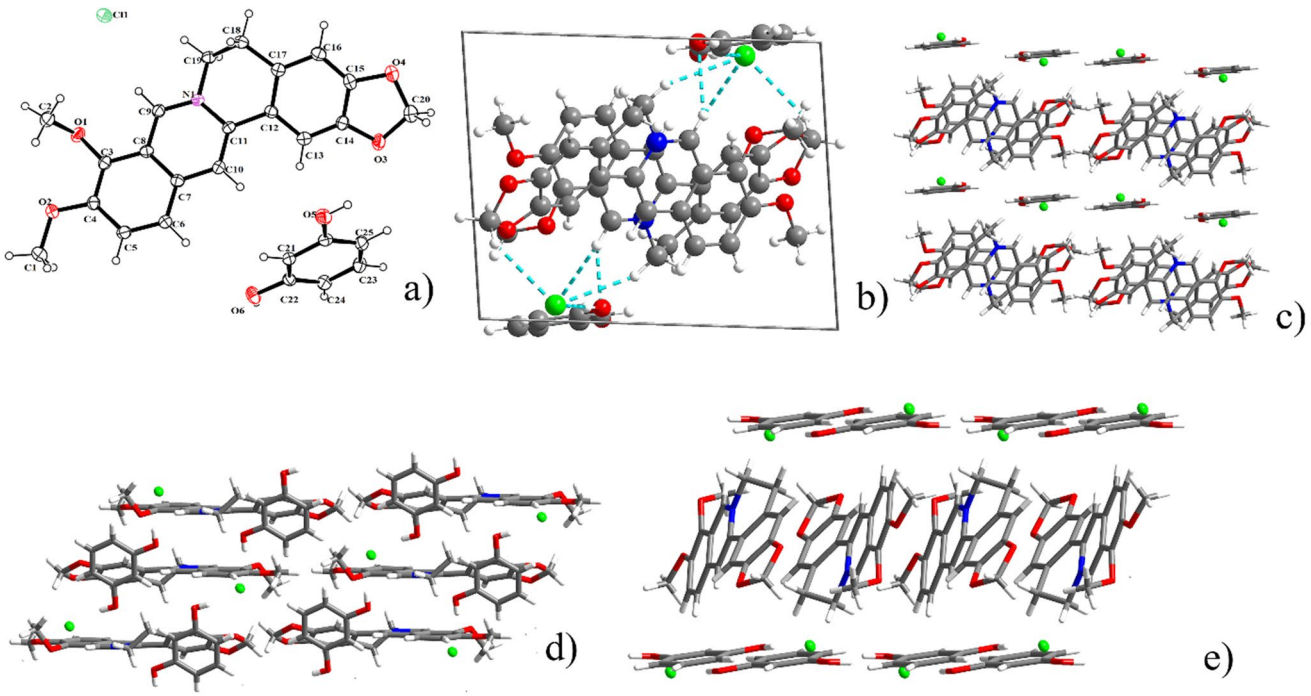

Fig. 3 The crystal structure of BCl-RES, (**a**) ORTEP diagram with labelling scheme, (**b**) key intermolecular interactions (hydrogen bonds are teal colored), and molecular packing viewed along (**c**) *a*-axis, (**d**) *b*-axis, and (**e**) *c*-axis.

CAT molecules pack to form a column running along the *b*-axis direction with chloride anions adjacent to berberine cations to maintain charge neutrality (Fig. 2b). Within each column, neighboring berberine molecules are related by an inversion center. Two berberine columns sandwich a column of CAT and H_2O (Fig. 2b). Each chloride anion connects to one CAT molecule through an O-H···Cl^- hydrogen bond, two H_2O molecules through two bifurcated O-H···Cl^- hydrogen bonds, and one berberine cation through two bifurcated C-H···Cl^- weak hydrogen bonds. Each H_2O molecule connects to an adjacent CAT molecule through an O-H···O hydrogen bond, and each CAT molecule connects to a berberine cation through a C-H···O hydrogen bond (Fig. 2b). Crystal structure viewed along the three unit cell axes are shown in Fig. 2c-e. Hydrogen bonds in BCl-CAT·H_2O are summarized in Table S1.

The asymmetric unit of BCl-RES contains one BCl and one RES (Fig. 3a). Berberine cations stack to form a column running along the *a*-axis direction with chloride anions in the neighborhood to maintain charge neutrality (Fig. 3b). Within each berberine column, the adjacent berberine cations are related through an inversion center. The RES molecules take an orientation with its molecular plane running parallel to the berberine columns, i.e., the *a*-axis (Fig. 3c). Each chloride anion connects to two RES molecules through two O-H···Cl^- hydrogen bonds and with three surrounding berberine cations through C-H···Cl^- weak hydrogen bonds. Each RES molecule connects with one berberine cation through a C-H···O hydrogen bond (Fig. 3b). Structure views along different unit cell axes are shown in Fig. 3c–e. Hydrogen bonds in BCl-RES are summarized in Table S2.

The asymmetric unit of BCl-HYQ·$CHCl_3$ contains two molecules of BCl, two molecules of $CHCl_3$, one whole molecule of HYQ and two half molecules of HYQ (Fig. 4a). Key interactions are graphically shown in Fig. 4b. Like the two earlier cocrystals, berberine cations stacked to form a column running along the *a*-axis direction (Fig. 4c) and adjacent berberine cations within each column are related through an inversion center. The presence of chlorine anion near berberine cations maintains the charge neutrality of the cocrystal. HYQ molecules, with a planar orientation parallel to the berberine columns, fill the space between berberine columns (Fig. 4b). Each HYQ molecule connects

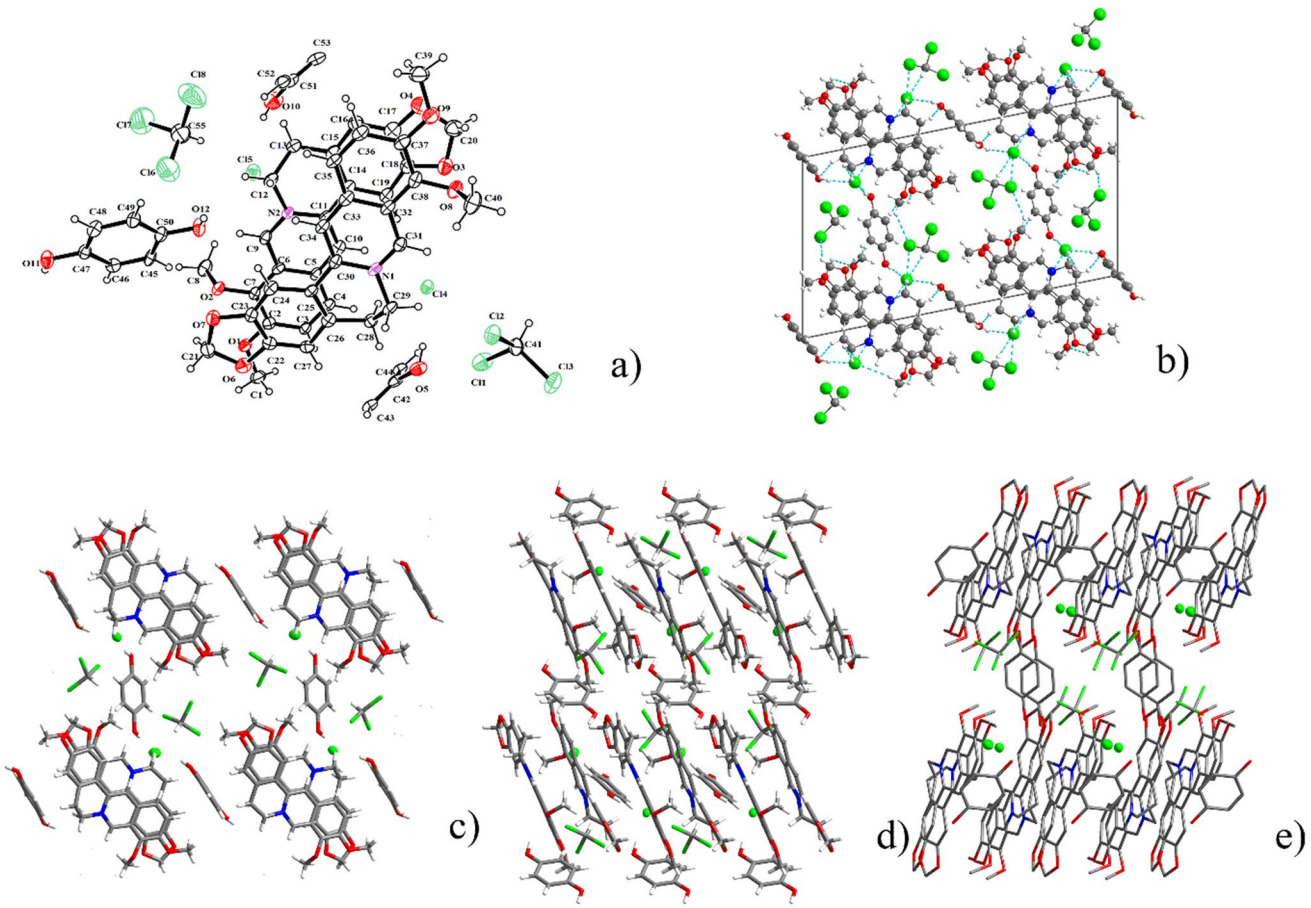

Fig. 4 The crystal structure of BCl-HYQ·$CHCl_3$, (**a**) ORTEP diagram with labelling scheme, (**b**) key intermolecular interactions (hydrogen bonds are teal colored), and molecular packing viewed along (**c**) *a*-axis, (**d**) *b*-axis, and (**e**) *c*-axis.

to two chloride anions through two O-H···Cl^- hydrogen bonds and two berberine cations through two C-H···O hydrogen bonds. Each chloride anion connects to a berberine cation through a C-H···Cl^- weak hydrogen bond. Each $CHCl_3$ molecule connects with one chloride anion through a C-H···Cl^- weak hydrogen bond and with two berberine cations through two bifurcated C-H···Cl^- weak hydrogen bonds (Fig. 4b). The structure of this crystal along different unit cell axes are shown in Fig. 4c–e. Hydrogen bonds in BCl-HYQ·$CHCl_3$ are summarized in Table S3.

PXRD Analysis

All of the three cocrystals exhibited characteristic diffraction peaks different from BCl·$2H_2O$, and characteristic peaks of initial components disappeared in their PXRD patterns (Fig. 5), which indicated the formation of three new crystalline phases. In addition, the PXRD patterns of three powders are in good agreement with the PXRD patterns calculated from the solved crystal structures, suggesting they are the same phase as these single crystals.

Thermal Analysis

The DSC thermogram of BCl·$2H_2O$ exhibited two endothermic peaks at ~87℃ and ~191℃ (Fig. 6), which correspond to dehydration of BCl·$2H_2O$ and melting of the anhydrous BCl, respectively.

Three endothermic peaks of ~110℃, 173℃ and 199℃ were observed in the DSC thermogram of BCl-CAT·H_2O (Fig. 6a). TGA data suggests that BCl-CAT·H_2O undergoes a weight loss of 3.69% when heated from room temperature to 120℃ (Fig. 6b), which is approximately that of the theoretical water content of 3.60%. Therefore, the broad endotherm peaked at 110℃ in the DSC thermogram corresponds to dehydration. Since the endothermic peak at 173℃ is not accompanied by any weight loss, it is attributed to the melting of anhydrous BCl-CAT. The sharp endothermic peak at 199℃, which corresponds to a significant weight loss, is attributed to thermal decomposition.

The DSC curve of BCl-RES showed a single melting endothermic peak at 207℃, which is accompanied by significant weight loss (Fig. 6). Hence, we attribute this to melting with simultaneous evaporation or degradation of the melt.

For BCl-HYQ·$CHCl_3$, the DSC thermogram exhibited three endothermic peaks at ~87℃, 151℃ and 224℃ (Fig. 6a). The first endotherm is interpreted as the loss

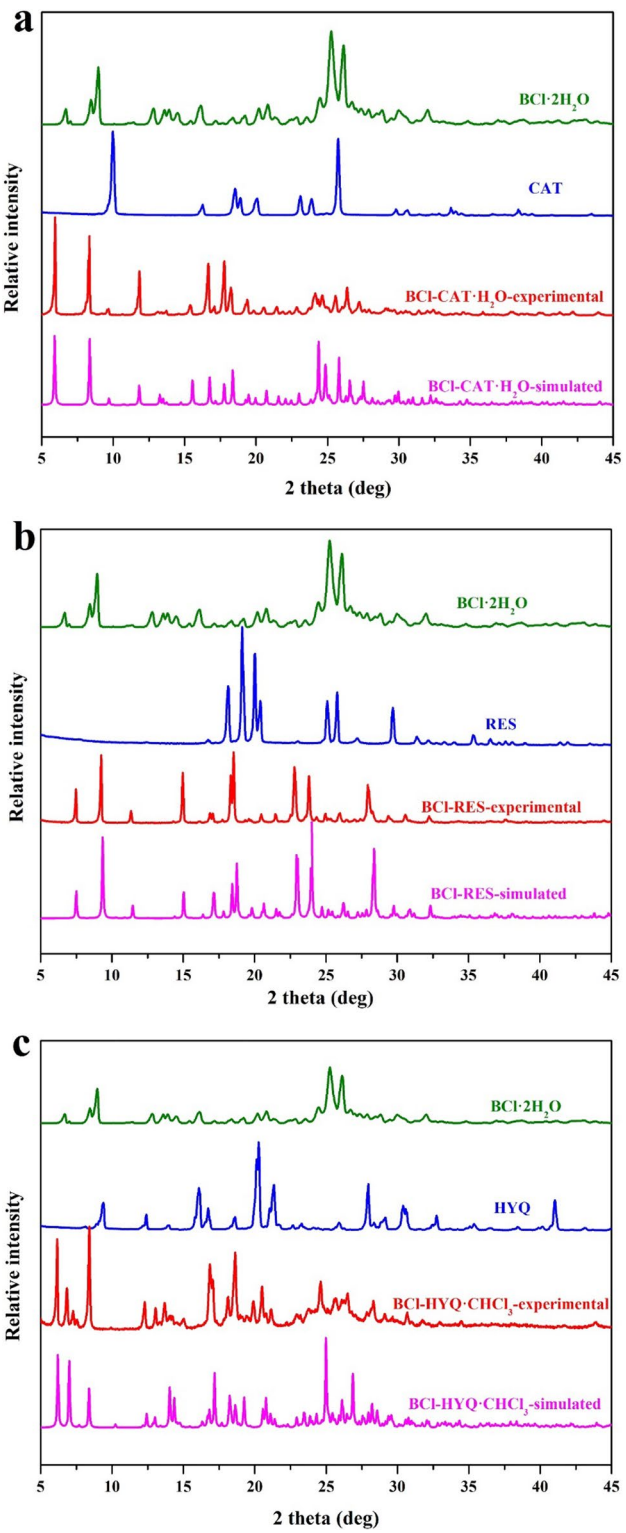

Fig. 5 Experimental and calculated PXRD patterns of (**a**) BCl-CAT·H_2O, (**b**) BCl-RES and (**c**) BCl-HYQ·$CHCl_3$ cocrystal powders compared with corresponding parent materials.

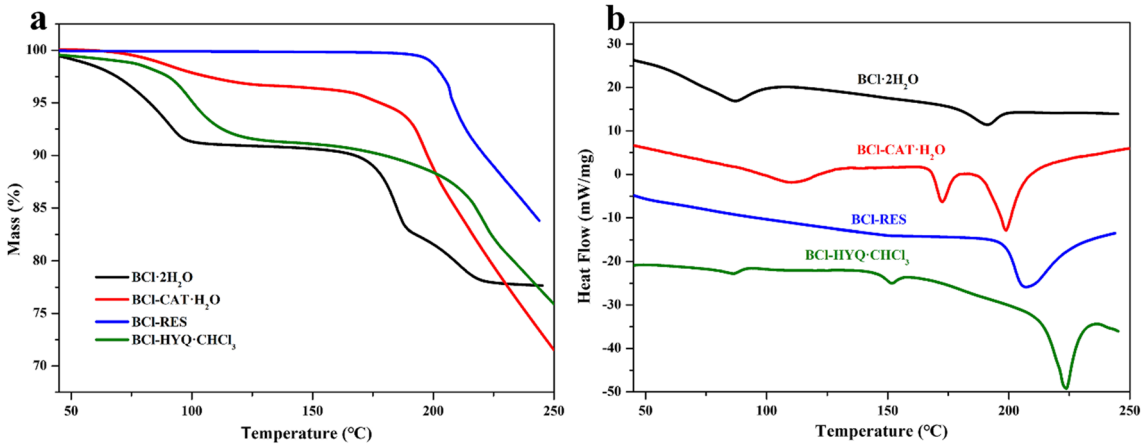

Fig. 6 TGA (**a**) and DSC (**b**) thermograms of BCl·2H_2O, BCl-CAT·H_2O, BCl-RES, and BCl-HYQ·$CHCl_3$.

of chloroform since it corresponds to a weight loss from room temperature to 100℃ (Fig. 6b). This weight loss (8.5%) is significantly lower than the theoretical chloroform content in the crystals (19.9%), indicating partial desolvation of the sample during storage. The endotherm at 151℃ is likely a polymorph phase change of the anhydrous BCl-HYQ since no weight change around that temperature. The endotherm at 223.8℃ is interpreted as melting accompanied by the decomposition of anhydrous BCl-HYQ. Overlaid TGA and DSC thermograms of BCl-2H_2O, along with each cocrystal and corresponding coformer are shown in Fig. S1.

FT-IR Spectroscopic Analysis

Figure 7 shows the FTIR spectra of BCl-CAT·H_2O, BCl-RES, BCl-HYQ·$CHCl_3$ cocrystals. The wave number assignments of main functional groups are summarized in

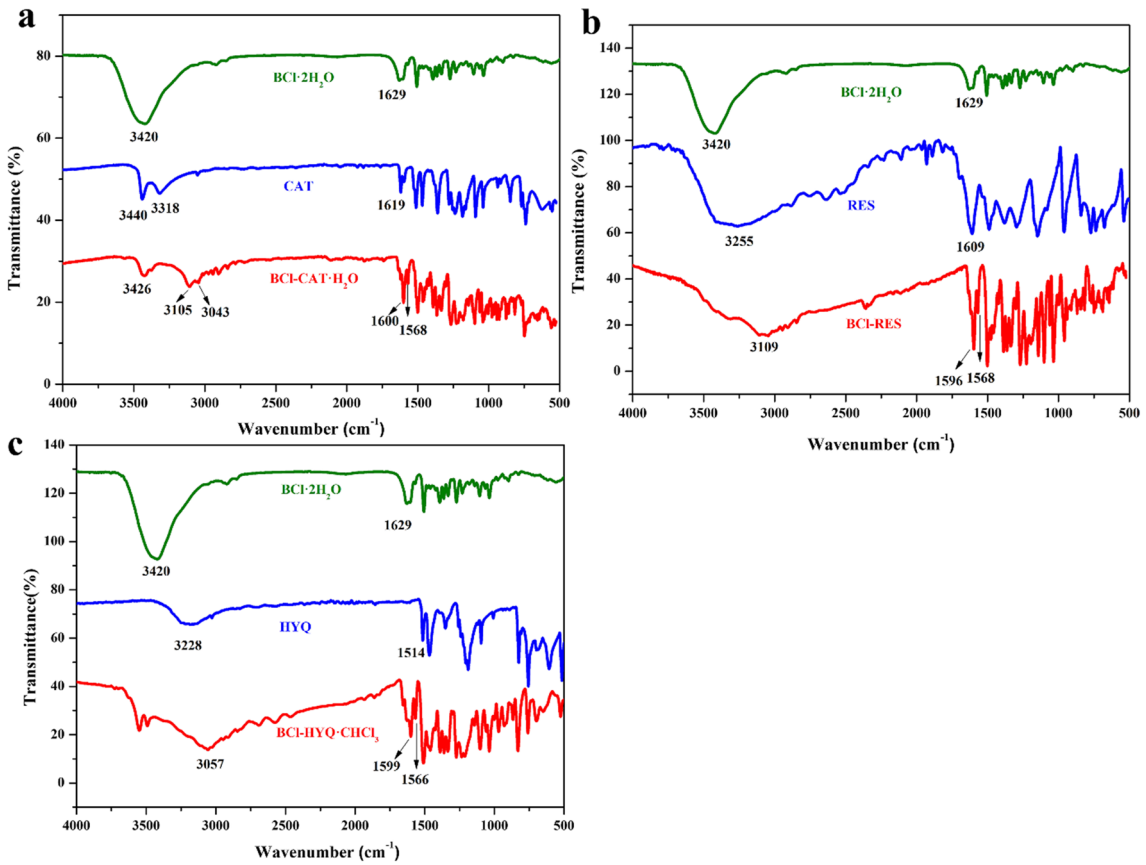

Fig. 7 FTIR spectra of (**a**) BCl-CAT·H_2O, (**b**) BCl-RES, (**c**) BCl-HYQ·$CHCl_3$ cocrystals.

Table II Assignments of Key FTIR Peaks of BCl·2H_2O, Cocrystals, and Coformers

Sample	νO-H	νC=C
BCl·2H_2O	3420	1629
CAT	3440/3318	1619
RES	3255	1609
HYQ	3228	1514
BCl-CAT·H_2O	3426/3105/3043	1600/1568
BCl-RES	3109	1596/1568
BCl-HYQ·$CHCl_3$	3057	1599/1566

Table II. In the FT-IR spectrum of BCl-CAT·H_2O, the strong absorption bands at 3440 cm^{-1} and 3318 cm^{-1} correspond to the O-H stretching vibrations, and the absorption band at 1619 cm^{-1} represents the stretching vibration of C=C of benzene ring of CAT. These absorption bands shifted to 3105 cm^{1}, 3043 cm^{-1} and 1568 cm^{-1}, respectively. The absorption band at 3426 cm^{-1} of BCl-CAT·H_2O correspond to the O-H stretching vibrations of water in the crystal lattice. In addition, the C=C stretching vibration at 1629 cm^{-1} for BCl·2H_2O is shifted to 1596 cm^{-1} in BCl-CAT·H_2O.

The absorption bands at 3255 cm^{-1} and 1609 cm^{-1} of RES are attributed to the stretching vibrations of O-H and C=C, respectively. They shift to 3109 (O-H) and 1568 cm^{-1} (C=C) in BCl-RES. The C=C stretching vibration of BCl·2H_2O (1629 cm^{-1}) shift to 1596 cm^{-1} in BCl-RES. In BCl-HYQ·$CHCl_3$, stretching vibrations of O-H (3228 cm^{-1}) and C=C (1514 cm^{-1}) of HYQ shift to 3057 cm^{-1} and 1566 cm^{-1}, respectively. In addition, the C=C stretching vibration for BCl·2H_2O at 1629 cm^{-1} shifted to 1599 cm^{-1} in the cocrystal. The shifts of stretching vibrations of various functional groups observed in cocrystals indicate the presence of intermolecular interactions between the BCl and coformers.

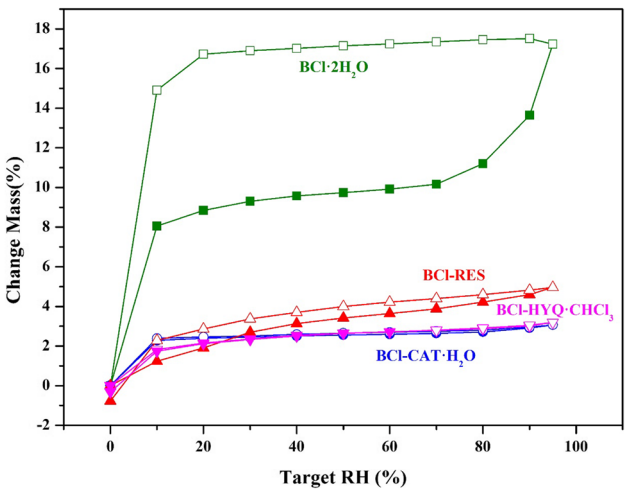

Fig. 8 DVS isotherms of BCl and three cocrystals at 25℃.

Hygroscopicity

Similar to a previous study [18], BCl absorbs 8.1% water at 10% RH to form a dihydrate (Fig. 8), which has a theoretical water content of 8.8%. Little weight change was observed in the RH range of 10%-70%, indicating physical stability of the dihydrate in this RH range. However, the weight increased sharply with RH above 80% and reached a water content of 17.2% at 95% RH, corresponding to a tetrahydrate (16.3% theoretical water content). The tetrahydrate remained stable when the RH decreased to 20%, but partial weight loss occurred at 10% RH and complete weight loss occurred at 0% RH.

All three cocrystals exhibited much lower hygroscopicity than BCl, with no more than 5% weight gained at 95% RH (Fig. 8). The dried BCl-CAT·H_2O attained 2.3% weight at 10% RH, roughly corresponding to one H_2O molecule (theoretical water content is 3.6%), indicating facile hydrate formation. The total weight gain eventually reached 3.1% at 95% RH. Since the overall weight gain was lower than that expected for a monohydrate, the initial drying step likely did not completely remove water from the crystal lattice of BCl-CAT·H_2O. However, the desorption curve superimposes the sorption curve with no observed hysteresis, suggesting excellent reversibility of the hydration and dehydration reactions and the isotherm corresponds to true thermodynamic equilibrium.

At 95% RH, the maximum amount of moisture gained was 4.7% by BCl-RES and 3.2% by BCl-HYQ·$CHCl_3$. Since their desorption curves were close to their sorption curve and no step changes in the isotherms, the weight gain is attributed to surface water adsorption. All three cocrystals fall in the "hygroscopic" class according to the classification in the European Pharmacopoeia (2–15% moisture uptake).

The PXRD patterns of the three cocrystals before and after the moisture sorption experiments suggest no phase change (Figure S2).

Solubility

BCl-CAT·H_2O and BCl-RES exhibited slightly higher aqueous solubility than BCl·2H_2O (Table III). However, the solubility of BCl-HYQ·$CHCl_3$ was slightly lower than BCl·2H_2O, i.e., 0.327 mg/mL at 37℃, which was measured after 3 days

Table III Solubility Values of BCl·2H_2O and Three Cocrystals at 37℃ ($n=3$)

Crystal form	Solubility (mg/mL)
BCl·2H_2O	3.10±0.03
BCl-CAT·H_2O	3.70±0.08
BCl-RES	3.93±0.13
BCl-HYQ·$CHCl_3$	2.89±0.03

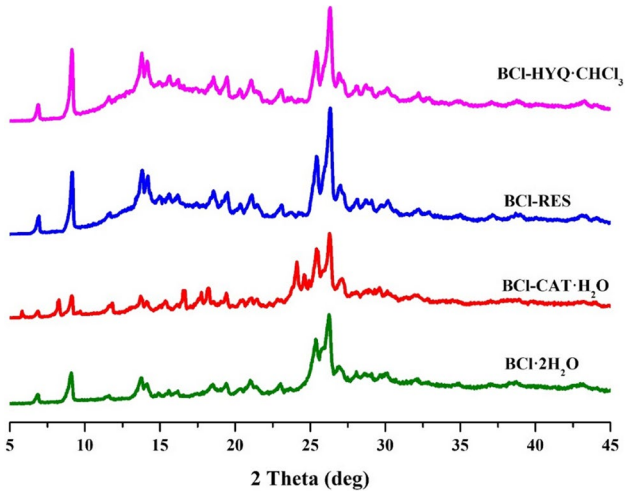

Fig. 9 PXRD patterns of $BCl{\cdot}2H_2O$ and three cocrystals after solubility experiment.

of equilibration in water [22]. The solubility values of cocrystals followed the descending order of BCl-RES > BCl-CAT·H_2O > BCl-HYQ·$CHCl_3$, which is the same as that of coformers, i.e., RES (1100 mg/mL) [26] > CAT (430 mg/mL) [26] > HYQ (70 mg/mL) [33].

PXRD analyses of solids at the end of the solubility experiments suggested complete transformation into $BCl{\cdot}2H_2O$ by BCl-RES and BCl-HYQ·$CHCl_3$ and partial transformation into $BCl{\cdot}2H_2O$ by BCl-CAT·H_2O (Fig. 9). Thus, the solubility values in Table III are merely reminiscent of the thermodynamic solubility of cocrystals, which should have been much more different from that of $BCl{\cdot}2H_2O$ had phase conversion not occurred. To mitigate the phase conversion issue during solubility measurements, we determined intrinsic dissolution rates of these crystals.

Dissolution Properties

All three cocrystals exhibited higher intrinsic dissolution rates (IDR) than that of $BCl{\cdot}2H_2O$ in water at 37℃ (Fig. 10a). The IDRs of the three cocrystals are 1.64, 5.42, 1.54 times higher than $BCl{\cdot}2H_2O$, following the descending order of BCl-RES (1.217 ± 0.007 mg/cm^2/min) > BCl-CAT·H_2O (0.367 ± 0.003 mg/cm^2/min) > BCl-HYQ·$CHCl_3$·(0.346 ± 0.005 mg/cm^2/min) > $BCl{\cdot}2H_2O$ (0.224 ± 0.002 mg/cm^2/min). The powder dissolution profiles are qualitatively consistent with the significantly different IDRs, where the time to complete dissolution follows the ascending order of BCl-RES (5 min) < BCl-CAT·H_2O (10 min) < BCl-HYQ·$CHCl_3$ (60 min) < $BCl{\cdot}2H_2O$ (120 min). Although BCl-CAT·H_2O and BCl-HYQ·$CHCl_3$ had similar IDR (Fig. 10a), BCl-HYQ·$CHCl_3$ did not disperse as easily as BCl-CAT·H_2O and formed lumps during powder dissolution. Thus, the effective surface area of BCl-HYQ·$CHCl_3$ is smaller, leading to slower powder dissolution (Fig. 10b). The significantly faster dissolution of all three cocrystals than $BCl{\cdot}2H_2O$ indicated their potential in improving the bioavailability of berberine. Of course, BCl-HYQ·$CHCl_3$ would not be suitable for use in commercial tablets due to the toxicity of $CHCl_3$.

Our results suggest that cocrystallization could be an effective approach for simultaneously modulating multiple pharmaceutical problems of berberine. Overall, BCl-RES is the best among the three cocrystals for use in tablet formulation because of its thermal stability, physical stability against RH variations, higher aqueous solubility, and faster dissolution. Also importantly, these new cocrystals expand the structure landscape of BCl solid forms, which is important for future analysis to attain a reliable relationship between crystal structure and pharmaceutical properties.

Conclusion

Three cocrystals of BCl with CAT, RES and HYQ were successfully prepared by the solvent evaporation method. Compared to $BCl{\cdot}2H_2O$, all three cocrystals exhibited better physical stability against high humidity and faster dissolution. These findings add to the existing evidence that

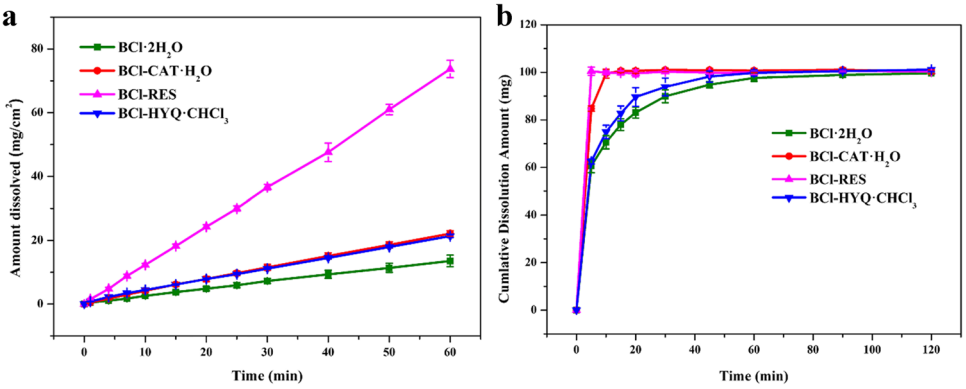

Fig. 10 Dissolution curves of $BCl{\cdot}2H_2O$, BCl-CAT·H_2O, BCl-RES, and BCl-HYQ·$CHCl_3$ in water at 37℃. (**a**) intrinsic dissolution rate, and (**b**) powder dissolution.

confirms the beneficial role of cocrystallization in facilitating drug development by improving multiple pharmaceutical properties. Among the three novel cocrystals, BCl-RES exhibits overall superior properties that make it a suitable solid form for developing a berberine oral tablet product.

Supplementary Information The online version contains supplementary material available at https://doi.org/10.1007/s11095-023-03533-w.

Declarations

Conflicts of Interests The authors declare no competing interest.

References

1. Shaikh R, Singh R, Walker GM, Croker DM. Pharmaceutical cocrystal drug products: an outlook on product development. Trends Pharmacol Sci. 2018;39:1033–48.
2. Kumari N, Ghosh A. Cocrystallization: cutting edge tool for physicochemical modulation of active pharmaceutical ingredients. Curr Pharm Des. 2020;26:4858–82.
3. Bavishi DD, Borkhataria CH. Spring and parachute: how cocrystals enhance solubility. Prog Cryst Growth Ch. 2016;62:1–8.
4. Desiraju GR. Crystal engineering: from molecule to crystal. J Am Chem Soc. 2013;135:9952–67.
5. Brittain HG. Pharmaceutical cocrystals: the coming wave of new drug substances. J Pharm Sci. 2013;102:311–7.
6. Dalpiaz A, Pavan B, Ferretti V. Can pharmaceutical co-crystals provide an opportunity to modify the biological properties of drugs? Drug Discov Today. 2017;22:1134–8.
7. Wang Y, Zhu W, Du W, Liu X, Zhang X, Dong H, *et al*. Cocrystals strategy towards materials for near-infrared photothermal conversion and imaging. Angew Chem Int Ed Engl. 2018;57:3963–7.
8. Saha S, Desiraju GR. Acid...Amide supramolecular synthon in cocrystals: from spectroscopic detection to property engineering. J Am Chem Soc. 2018;140(20):6361–73.
9. Sun L, Zhu W, Zhang X, Li L, Dong H, Hu W. Creating organic functional materials beyond chemical bond synthesis by organic cocrystal engineering. J Am Chem Soc. 2021;143:19243–56.
10. Aakeröy CB, Salmon DJ. Building co-crystals with molecular sense and supramolecular sensibility. CrystEngComm. 2005;7:439–48.
11. Sun CC. Materials science tetrahedron–a useful tool for pharmaceutical research and development. J Pharm Sci. 2009;98:1671–87.
12. Chu M, Ding R, Chu Z-y, Zhang M-b, Liu X-y, Xie S-h, *et al*. Role of berberine in anti-bacterial as a high-affinity LPS antagonist binding to TLR4/MD-2 receptor. BMC Complem Altern M. 2014; 14:89.
13. Zou K, Li Z, Zhang Y, Zhang HY, Li B, Zhu WL, *et al*. Advances in the study of berberine and its derivatives: a focus on anti-inflammatory and anti-tumor effects in the digestive system. Acta Pharmacol Sin. 2017;38:157–67.
14. Ma Y-G, Liang L, Zhang Y-B, Wang B-F, Bai Y-G, Dai Z-J, *et al*. Berberine reduced blood pressure and improved vasodilation in diabetic rats. J Mol Endocrinol. 2017;59:191–204.
15. Song D, Hao J, Fan D. Biological properties and clinical applications of berberine. Front Med. 2020;14:564–82.
16. Wang LH, Yu CH, Fu Y, Li Q, Sun YQ. Berberine elicits antiarrhythmic effects via IK1/Kir2.1 in the rat type 2 diabetic myocardial infarction model. Phytother Res. 2011; 25:33–7.
17. Lu Q, Dun J, Chen JM, Liu S, Sun CC. Improving solid-state properties of berberine chloride through forming a salt cocrystal with citric acid. Int J Pharm. 2019;554:14–20.
18. Wang L, Liu S, Gao Z. Crystal structure, dissolution and hygroscopicity of a novel cocrystal hydrate of berberine hydrochloride with L(+)-lactic acid. Pharmazie. 2020;75:483–7.
19. Wang L, Liu S, Chen JM, Wang YX, Sun CC. Novel salt-cocrystals of berberine hydrochloride with aliphatic dicarboxylic acids: odd-even alternation in physicochemical properties. Mol Pharm. 2021;18:1758–67.
20. Gao Z, Liu S, Sun CC. Complexation with aromatic carboxylic acids expands the solid-state landscape of berberine. Int J Pharm. 2022;617: 121587.
21. Yang D, Cao J, Jiao L, Yang S, Zhang L, Lu Y, *et al*. Solubility and stability advantages of a new cocrystal of berberine chloride with fumaric acid. ACS Omega. 2020;5(14):8283–92.
22. Tong HHY, Chow ASF, Chan HM, Chow AHL, Wan YKY, Williams ID, Shek FLY, Chan CK. Process-induced phase transformation of berberine chloride hydrates. J Pharm Sci. 2010;99:1942–54.
23. Childs SL, Chyall LJ, Dunlap JT, Smolenskaya VN, Stahly BC, Stahly GP. Crystal engineering approach to forming cocrystals of amine hydrochlorides with organic acids. Molecular Complexes of fluoxetine hydrochloride with benzoic, succinic, and fumaric acids. J Am Chem Soc. 2004; 126:13335–42.
24. Hong C, Xie Y, Yao Y, Li G, Yuan X, Shen H. A novel strategy for pharmaceutical cocrystal generation without knowledge of stoichiometric ratio: myricetin cocrystals and a ternary phase diagram. Pharm Res. 2015;32:47–60.
25. Good DJ, Rodríguez-Hornedo N. Solubility advantage of pharmaceutical cocrystals. Cryst Growth Des. 2009;9:2252–64.
26. Bolla G, Sanphui P, Nangia A. Solubility advantage of tenoxicam phenolic cocrystals compared to salts. Cryst Growth Des. 2013;13:1988–2003.
27. Luo Y-H, Sun B-W. Pharmaceutical co-crystals of pyrazinecarboxamide (PZA) with various carboxylic acids: crystallography, hirshfeld surfaces, and dissolution study. Cryst Growth Des. 2013;13:2098–106.
28. Maddileti D, Jayabun SK, Nangia A. Soluble cocrystals of the xanthine oxidase inhibitor febuxostat. Cryst Growth Des. 2013;13:3188–96.
29. Sanphui P, Goud NR, Khandavilli UBR, Nangia A. Fast dissolving curcumin cocrystals. Cryst Growth Des. 2011;11:4135–45.
30. Karki S, Friščić T, Fábián L, Jones W. New solid forms of artemisinin obtained through cocrystallisation. CrystEngComm. 2010;12:4038–41.
31. Gangavaram S, Raghavender S, Sanphui P, Pal S, Manjunatha SG, Nambiar S, *et al*. Polymorphs and cocrystals of nalidixic acid. Cryst Growth Des. 2012;12:4963–71.
32. Wong SN, Hu S, Ng WW, Xu X, Lai KL, Lee WYT, *et al*. Cocrystallization of curcumin with benzenediols and benzenetriols via rapid solvent removal. Cryst Growth Des. 2018;18:5534–46.
33. Goud NR, Suresh K, Sanphui P, Nangia A. Fast dissolving eutectic compositions of curcumin. Int J Pharm. 2012;439:63–72.